

A Hybrid Phase-Flow Method for Hamiltonian Systems with Discontinuous Hamiltonians *

Shi Jin[†], Hao Wu[‡] and Zhongyi Huang[§]

August 26, 2008

Abstract

In this paper, we propose a new phase flow method for Hamiltonian systems with discontinuous Hamiltonians. In the original phase-flow method introduced by Ying and Candès [26], the phase map should be smooth to ensure the accuracy of the interpolation. Such an interpolation is inaccurate if the phase map is nonsmooth, for example, when the Hamiltonian is discontinuous. We modify the phase flow method using a discontinuous Hamiltonian solver, and establish the stability (for piecewise constant potentials) of such a solver. This extends the applicability of the highly efficient phase flow method to singular Hamiltonian systems, with a mild increase of algorithm complexity. Such a particle method can be useful for the computation of high frequency waves through interfaces.

Key words: phase-flow method, particle method, discontinuous Hamiltonian, interface, high frequency waves, Liouville equation

Contents

1	Introduction	2
2	The Discontinuous Hamiltonian systems	3
2.1	The behavior of a classical particle at a potential barrier . . .	3
2.2	A discontinuous Hamiltonian system solver and its stability .	5
2.3	A numerical solver for the discontinuous Hamiltonian system	8

*This work was partially supported by NSF grant No. DMS-0608720, NSFC Projects 10676017, the National Basic Research Program of China under the grant 2005CB321701. SJ was also supported by a Van Vleck Distinguished Research Prize from University of Wisconsin-Madison.

[†]Department of Mathematics, University of Wisconsin, Madison, WI 53706-1388, USA (jin@math.wisc.edu).

[‡]Department of Mathematical Sciences, Tsinghua University, Beijing, 10084, China (hwu04@mails.tsinghua.edu.cn)

[§]Department of Mathematical Sciences, Tsinghua University, Beijing, 10084, China (zhuang@math.tsinghua.edu.cn)

3	The Hybrid Phase-Flow Method	9
3.1	The hybrid phase flow method	9
3.2	The detailed implementation	10
4	Applications and numerical examples	13
5	Conclusion	22

1 Introduction

We are interested in an efficient and accurate numerical method for the Hamiltonian system

$$\frac{d\mathbf{x}}{dt} = \nabla_{\boldsymbol{\xi}} H, \quad (1)$$

$$\frac{d\boldsymbol{\xi}}{dt} = -\nabla_{\mathbf{x}} H, \quad (2)$$

where $\mathbf{x} = \mathbf{x}(t) : \mathbb{R} \rightarrow \mathbb{R}^d$, $\boldsymbol{\xi} = \boldsymbol{\xi}(t) : \mathbb{R} \rightarrow \mathbb{R}^d$ are particle position and velocity at time t respectively, while the Hamiltonian $H = H(\mathbf{x}, \boldsymbol{\xi}) : \mathbb{R}^{2d} \rightarrow \mathbb{R}$ is piecewise smooth with finitely many discontinuities. Such a problem arises in classical particles through media that contain barriers or interfaces at which the Hamiltonian is discontinuous. It also arises as the Lagrangian description of geometrical optics, or more generally, in the high frequency limit of linear high frequency waves, through interfaces.

If H is smooth, then (1)-(2) can be solved using classical theory of ordinary differential equations for any given initial condition

$$\mathbf{x}(0) = \mathbf{x}_0, \boldsymbol{\xi}(0) = \boldsymbol{\xi}_0. \quad (3)$$

At time $t = T$, we define the solution by

$$H_T(\mathbf{x}_0, \boldsymbol{\xi}_0) = (\mathbf{x}(T; \mathbf{x}_0, \boldsymbol{\xi}_0), \boldsymbol{\xi}(T; \mathbf{x}_0, \boldsymbol{\xi}_0)), \quad (4)$$

which is a flow (or map) on the initial data $(\mathbf{x}_0, \boldsymbol{\xi}_0)$. The system can be solved numerically by a standard numerical method, or a symplectic scheme [19]. If one needs to treat many initial data at the same time, one can use the phase-flow method, introduced by Ying and Candès [26], to significantly increase the computational speed. For example, if \tilde{N} particles are to be simulated for L time steps, a typical ODE solver for system (1)-(2) has a computational cost of $O(\tilde{N}L)$, while the phase-flow method has a cost of $O(\tilde{N}L^{1/K})$, here K denotes the number of iterative steps.

However, if H is only piecewise smooth, with finite number of discontinuities, the aforementioned approaches face difficulties. First, the underlying Hamiltonian system, or the system of ODEs, (1)-(2), does not have the classical notion of solution and well-posedness for the initial value problem,

which requires the right hand side to be at least Lipschitz continuous. For the right hand side to have only bounded variation, one can use the notion of renormalized solution to define the weak solutions [3, 1]. When H is discontinuous, all these theories do not apply.

In [14, 15, 17] (see also [10]), a notion of solution was introduced for singular Hamiltonian system (1)-(2). The idea is to define its solution at an interface using particle transmission and reflection. Depending on the momentum of the particle versus the potential jump, the particle can be either reflected or transmitted. This defines a physically relevant solution to the singular system (1)-(2). Corresponding numerical schemes can then be designed which yield convergent solutions to such singular Hamiltonian systems.

In this paper, we first prove the stability with respect to initial data on so-defined solutions for piecewise constant potentials, and then combine such a solver with the phase-flow method, which results in a fast solver for singular Hamiltonian systems for the numerical simulation of many classical particles. Since the phase flow method needs to use local interpolations on particle position and velocity, it requires certain regularity on the solutions in order to achieve desired numerical accuracy. Our system, unfortunately, admits *discontinuous* solutions which cannot be interpolated using classical interpolation techniques. For particles undergoing transmissions and reflections, which result in discontinuous solutions, instead of using local interpolations, we will use the numerical Hamiltonian solver directly. We refer to our approach as the *hybrid phase-flow method*. Our method will increase the computational cost than the original phase-flow method designed for smooth Hamiltonians. Nevertheless, since the particles undergoing transmissions and reflections, thus requiring special treatments, are in small numbers compared to the total number of particles, the increased computational cost is minor.

The paper is organized as follows. In Section 2, after describing the behavior of a classical particle at a potential barrier, we recall the discontinuous Hamiltonian solver introduced in [14, 17], and prove its stability (for piecewise constant potentials) with respect to the initial data. The hybrid phase-flow method is given in Section 3. In Section 4, numerical examples are presented to study the accuracy and efficiency of the proposed method. We conclude the paper in Section 5.

2 The Discontinuous Hamiltonian systems

2.1 The behavior of a classical particle at a potential barrier

In classical mechanics, a particle will either cross a potential barrier with a changing momentum, or be reflected, depending on its momentum and on the strength of the potential barrier. The Hamiltonian $H = \frac{1}{2}|\xi|^2 + V(\mathbf{x})$

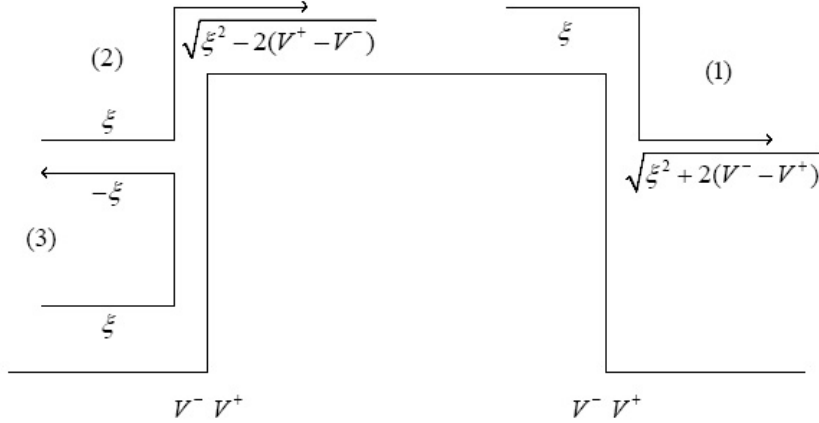


Figure 1: Change of particle momentum across a potential barrier for the case when $\xi^- > 0$.

should be conserved across the potential barrier:

$$\frac{1}{2}|\xi^-|^2 + V(\mathbf{x}^-) = \frac{1}{2}|\xi^+|^2 + V(\mathbf{x}^+) \quad (5)$$

where the superscripts \pm indicate the right and left limits of the quantity at the potential barrier.

To simplify the problem, we just consider the 1D case. (For the high dimension problems, we only need to deal with the normal direction at the potential barrier.) Consider the case when, at a potential barrier, the particle is moving into the barrier with a velocity $\xi^- > 0$. There are three possibilities (see Figure 1):

- 1) $V^- > V^+$. In this case, the potential decreases, so the particle will cross the potential barrier and gain momentum in order to maintain a constant Hamiltonian. (5) implies

$$\xi^+ = \sqrt{(\xi^-)^2 + 2(V^- - V^+)} \quad (6)$$

- 2) $V^- < V^+$ and $\frac{1}{2}(\xi^-)^2 > V^+ - V^-$. If the kinetic energy of the particle is bigger than the potential jump then the particle will cross the barrier with a reduced momentum. (5) implies

$$\xi^+ = \sqrt{(\xi^-)^2 - 2(V^+ - V^-)} \quad (7)$$

- 3) $V^- < V^+$ and $\frac{1}{2}(\xi^-)^2 < V^+ - V^-$. In this case, the kinetic energy is not large enough for the particle to cross the potential barrier, so the particle will be reflected with a negative velocity $-\xi^-$.

If $\xi^- < 0$, similar behavior can also be analyzed using the constant Hamiltonian condition (5).

2.2 A discontinuous Hamiltonian system solver and its stability

When V contains discontinuities, the initial value problem of the the Hamiltonian system (1)-(2) is not well-posed in the classical sense which requires the right hand side to be Lipschitz-continuous [9]. In [14, 16], such a singular Hamiltonian system was solved by incorporating the particle behavior at the barrier described in the preceding subsection. For the sake of simplicity and clarify, we describe the 1D case here. Consider the potential given by

$$V(x) = \begin{cases} V_1(x), & x < 0, \\ V_2(x), & x > 0. \end{cases} \quad (8)$$

Assume $V_1(x) \in C^2(-\infty, 0)$, $V_2(x) \in C^2(0, \infty)$, with finite limits at $x = 0$ for s derivatives ($s = 0, 1, 2$), i.e.

$$V_{(s)}^- = \lim_{x \rightarrow 0^-} V_1^{(s)}(x) < \infty, \quad V_{(s)}^+ = \lim_{x \rightarrow 0^+} V_2^{(s)}(x) < \infty. \quad (9)$$

Assume that in finite time, the particle will hit the barrier only finitely many times. Then the solution map $H_T : (x_0, \xi_0) \mapsto (x(T), \xi(T))$ can be written as a composition of the standard Hamiltonian solver $h_{k,t}$ and the interface solver \tilde{h} :

$$H_T = h_{t_p} \circ \tilde{h} \circ h_{t_{p-1}} \circ \tilde{h} \circ \dots \circ h_{t_2} \circ \tilde{h} \circ h_{t_1}, \quad (10)$$

with $T = \sum_{i=1}^p t_i$, where t_i is the time between two consecutive interactions of the particle with the barriers. Here the standard Hamiltonian solver h_t is defined within a smooth region of V .

Without loss of generality, we assume $[V] = V_{(0)}^+ - V_{(0)}^- > 0$. The case of a negative potential jump can be handled in the same fashion. The interface solver $\tilde{h} : L_1 \rightarrow L_2$ is given by

$$\tilde{h}(x, \xi) = \begin{cases} (0^-, -\xi), & x = 0^-, \xi > 0, \xi^2 < 2[V], \\ (0^+, \sqrt{\xi^2 - 2[V]}), & x = 0^-, \xi > 0, \xi^2 > 2[V], \\ (0^-, -\sqrt{\xi^2 + 2[V]}), & x = 0^+, \xi < 0, \end{cases} \quad (11)$$

where $L_1 = \{(0^+, \xi) | \xi < 0\} \cup \{(0^-, \xi) | \xi > 0\}$ is the set of particles at the barrier moving *toward* the barrier, while $L_2 = \{(0^+, \xi) | \xi > 0\} \cup \{(0^-, \xi) | \xi < 0\}$ is the set of particles at the barrier moving *away* from the barrier. Here \tilde{h} is a two component vector-function, $\tilde{h}(x, \xi) = (\tilde{h}^{(1)}(x, \xi), \tilde{h}^{(2)}(x, \xi))$. Clearly, $\tilde{h}^{(1)}(x, \xi) = x$ without ambiguity.

The solution to the singular Hamiltonian system (1)-(2) described by H_T is constructed as follows. Given the initial data, one solves the system using a standard Hamiltonian solver h_{t_1} for time duration t_1 which is the first time the particle hits the barrier. At $t = t_1$, one applies the interface map \tilde{h} to get the new initial data for the next standard Hamiltonian solver h_{t_2} and the process continues until the destination time.

We now justify the stability for initial value problem of this solution. We will only carry out the analysis for piecewise constant potentials,

$$V(x) = \begin{cases} V^-, & x < 0, \\ V^+, & x > 0, \end{cases} \quad (12)$$

If V is monotonely decreasing toward the barrier, then a similar argument can also imply the stability. The case of more general potentials is an interesting topic but will not be pursued here.

For the special potential (12), $\xi(t)$ will be piecewise constant, while $x(t)$ is piecewise linear.

We first prove the stability of the interface map \tilde{h} under some reasonable assumptions on the initial data so we can avoid the issue of critical direction $\xi_c^2 = 2[V]$, namely, we need to consider the domain $C = \{\xi_0 \in \mathbb{R} \mid |\xi_0^2 - 2[V]| > \epsilon_0\}$ with small parameter $0 < \epsilon_0 < 2[V]$, where $\xi_0 = \xi(0)$.

Lemma 1 *Consider the domain $L_c = \{(0^\pm, \xi) \in L_1 \mid \xi \in C\}$ of particles moving into the barrier, with the critical direction excluded. The interface map \tilde{h} is stable on L_c in the sense that, $\forall \delta_1 > 0, \exists \delta_2, 0 < \delta_2 < \sqrt{2[V] + \epsilon_0} - \sqrt{2[V] - \epsilon_0}$, such that $\forall (x, \xi), (y, \eta) \in L_c, x = 0^\pm, y = 0^\pm$,*

$$|\xi - \eta| < \delta_2 \Rightarrow |\tilde{h}^{(2)}(x, \xi) - \tilde{h}^{(2)}(y, \eta)| < \delta_1. \quad (13)$$

Proof: We do not discuss $\tilde{h}^{(1)}$ because \tilde{h} does not change x at $x = 0$ (although we have been using notations 0^\pm).

First note that since $\delta_2 < \sqrt{2[V] + \epsilon_0} - \sqrt{2[V] - \epsilon_0}$, (x, ξ) and (y, η) are in the same side of the barrier. Namely, they will both be transmitted or reflected. We discuss all three possibilities:

1. If $x = 0^-, 0 < \xi, \eta < \sqrt{2[V]}$ (both particles are reflected), then

$$\left| \tilde{h}^{(2)}(x, \xi) - \tilde{h}^{(2)}(y, \eta) \right| \leq |\xi - \eta| < \delta_2. \quad (14)$$

2. If $x = 0^-, \xi, \eta > \sqrt{2[V]}$ (both particles will be transmitted), then

$$\begin{aligned} \left| \tilde{h}^{(2)}(x, \xi) - \tilde{h}^{(2)}(y, \eta) \right| &= \left| \sqrt{\xi^2 - 2[V]} - \sqrt{\eta^2 - 2[V]} \right| \\ &= \frac{\xi + \eta}{\sqrt{\xi^2 - 2[V]} + \sqrt{\eta^2 - 2[V]}} |\xi - \eta|. \end{aligned} \quad (15)$$

Let $g(\xi, \eta) = \frac{\xi + \eta}{\sqrt{\xi^2 - 2[V]} + \sqrt{\eta^2 - 2[V]}} > 0$. A simple computation shows $g_\xi \leq 0, g_\eta \leq 0$ for $\xi, \eta > 0$. Therefore,

$$g(\xi, \eta) \leq g(\sqrt{2[V] + \epsilon_0}, \sqrt{2[V] + \epsilon_0}) = \sqrt{\frac{2[V] + \epsilon_0}{\epsilon_0}}, \quad (16)$$

and

$$\left| \tilde{h}^{(2)}(x, \xi) - \tilde{h}^{(2)}(y, \eta) \right| \leq \sqrt{\frac{2[V] + \epsilon_0}{\epsilon_0}} \delta_2. \quad (17)$$

3. If $x = 0^+$, $\xi, \eta < 0$, then both particles will cross the barrier, and

$$\begin{aligned} \left| \tilde{h}^{(2)}(x, \xi) - \tilde{h}^{(2)}(y, \eta) \right| &= \left| \sqrt{\xi^2 + 2[V]} - \sqrt{\eta^2 + 2[V]} \right| \\ &= \frac{|\xi + \eta|}{\sqrt{\xi^2 + 2[V]} + \sqrt{\eta^2 + 2[V]}} |\xi - \eta| \\ &\leq |\xi - \eta| < \delta_2. \end{aligned} \quad (18)$$

Finally, by taking

$$\delta_2 < \min \left\{ \sqrt{2[V] + \epsilon_0} - \sqrt{2[V] - \epsilon_0}, \sqrt{\frac{\epsilon_0}{2[V] + \epsilon_0}} \delta_1 \right\}, \quad (19)$$

one has

$$\left| \tilde{h}^{(2)}(x, \xi) - \tilde{h}^{(2)}(y, \eta) \right| < \delta_1. \quad (20)$$

This completes the proof.

Since the stability of h_t is standard, we can now obtain the stability of H_T after excluding the critical direction L_c and the zero velocity.

Theorem 1 *Consider two solutions $(x(t), \xi(t))$ and $(y(t), \eta(t))$ defined via the phase map H_t with initial data $(x(0), \xi(0)) = (x_0, \xi_0) \in D$ and $(y(0), \eta(0)) = (y_0, \eta_0) \in D$ where $D = \{ \xi_0 \mid |\xi_0^2 - 2[V]| > \epsilon_0, |\xi_0| > \epsilon_0 \}$ with small parameter $0 < \epsilon_0 < \sqrt{2[V]}$. Then the phase map H_t is stable on D . That is, $\forall \delta_1 > 0, \exists \delta_2(t) > 0$, such that*

$$|(x_0, \xi_0) - (y_0, \eta_0)| < \delta_2 \Rightarrow |(x(t), \xi(t)) - (y(t), \eta(t))| < \delta_1. \quad (21)$$

Proof: We will only consider the case in which $\xi_0 > \eta_0 > \epsilon_0, y_0 < x_0 < 0$, namely, both particles will move from the left side of the barrier toward the barrier. We will only consider the (most complicated) case where both particles have transmitted to the right side of the barrier. The other cases can be analyzed similarly and actually somewhat more easily.

Under our assumption, the particle $x(t)$ will pass the barrier first. Assume it takes time t_1 for $x(t)$ to reach the barrier, and time t_2 for particle $y(t)$ to hit the barrier, with $t_2 > t_1$. The analytical solution at $t > t_2$ is given by

$$\begin{aligned} x(t) &= \xi^+(t - t_1), & \xi(t) &= \xi^+, \\ y(t) &= \eta^+(t - t_2), & \eta(t) &= \eta^+, \end{aligned}$$

where $\xi^+ = \sqrt{\xi_0^2 - 2[V]}$, $\eta^+ = \sqrt{\eta_0^2 - 2[V]}$. Thus,

$$\begin{aligned} x(t) - y(t) &= \xi^+(t - t_1) - \eta^+(t - t_2) \\ &= \sqrt{\xi_0^2 - 2[V]}(t - t_1) - \sqrt{\eta_0^2 - 2[V]}(t - t_2) \\ &= \left(\sqrt{\xi_0^2 - 2[V]} - \sqrt{\eta_0^2 - 2[V]} \right) (t - t_1) \\ &\quad + \sqrt{\eta_0^2 - 2[V]}(t_2 - t_1) \end{aligned}$$

Note that

$$t_2 - t_1 = -y_0/\eta_0 + x_0/\xi_0. \quad (22)$$

Now the stability of \tilde{h} , and the assumption that $\xi_0, \eta_0 > \epsilon_0$, lead to the desired stability, which is a simple exercise and will be left for the readers.

Remark 1 *The stability was established in domain D , which excludes the critical angle $|\xi| = \sqrt{2[V]}$ or tangent angle $\xi = 0$. There are the angles where classical Hamiltonian system break down and we have to consider the diffraction [18].*

2.3 A numerical solver for the discontinuous Hamiltonian system

The construction of the map \tilde{h} motivates the construction of the following numerical solver $\Theta_{\Delta t}(\mathbf{x}, \boldsymbol{\xi}) : \mathbb{R}^{2d} \rightarrow \mathbb{R}^{2d}$ for the Hamiltonian system (1)-(2) with discontinuous potential, following the idea of [17]. To approximate the smooth map h_{t_i} in H_T , we use a second order symplectic solver $\Upsilon_{\Delta t}(\mathbf{x}, \boldsymbol{\xi}) : \mathbb{R}^{2d} \rightarrow \mathbb{R}^{2d}$, see for example [6, 19]. The discontinuous ODE solver is $(\mathbf{x}^{n+1}, \boldsymbol{\xi}^{n+1}) = \Theta_{\Delta t}(\mathbf{x}^n, \boldsymbol{\xi}^n)$ (see Figure 2):

1. Estimate the updated position of the particle $(\mathbf{x}^*, \boldsymbol{\xi}^*) = \Upsilon_{\Delta t}(\mathbf{x}^n, \boldsymbol{\xi}^n)$.
2. If \mathbf{x}^* is in the same region as \mathbf{x}^n , i.e., if the particle has not crossed the interface Γ during the time interval $[t^n, t^{n+1}]$, we set $(\mathbf{x}^{n+1}, \boldsymbol{\xi}^{n+1}) = (\mathbf{x}^*, \boldsymbol{\xi}^*)$.
3. If \mathbf{x}^* and \mathbf{x}^n are in different regions.
 - (a) Approximate the interface crossing time $\Delta t^* = \frac{d(\mathbf{x}^n)}{d(\mathbf{x}^*) + d(\mathbf{x}^n)} \Delta t$, where $d(\mathbf{x})$ is the distance to the interface.
 - (b) Estimate $(\mathbf{x}_{(1)}^*, \boldsymbol{\xi}_{(1)}^*) = \Upsilon_{\Delta t^*}(\mathbf{x}, \boldsymbol{\xi})$.
 - (c) Let $(\mathbf{x}^*, \boldsymbol{\xi}_{(2)}^*) = \tilde{h}(\mathbf{x}^*, \boldsymbol{\xi}_{(1)}^*)$.
 - (d) Let $(\mathbf{x}^{n+1}, \boldsymbol{\xi}^{n+1}) = \Upsilon_{\Delta t - \Delta t^*}(\mathbf{x}_{(1)}^*, \boldsymbol{\xi}_{(2)}^*)$.

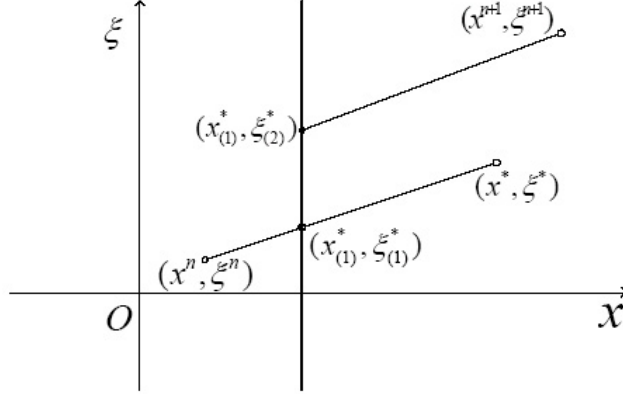


Figure 2: A graphic interpretation of the interface solver.

Remark 2 *The consistency error of discontinuous ODE solver is second order. It is based on two points: 1) the symplectic solver is of second order, 2) the interface crossing time Δt^* is estimated as second order. We will show that the solver $\Theta_{\Delta t}$ also converges at second order in numerical examples.*

3 The Hybrid Phase-Flow Method

3.1 The hybrid phase flow method

We first recall some basic terminology. For a fixed time t , the map $H_t : \mathbb{R}^{2d} \rightarrow \mathbb{R}^{2d}$ is called the phase map. The family $\{H_t : t \in \mathbb{R}\}$ of all phase maps defines the phase flow. The phase flow has a one parameter group structure, $H_{t_1} \circ H_{t_2} = H_{t_1+t_2}$, and the inverse of H_t is $H_t^{-1} = H_{-t}$. A manifold $M \subset \mathbb{R}^{2d}$ is said to be invariant if $H_t(M) \subset M$. We will consider the phase map H_t on an invariant manifold.

Similar to the phase-flow method, the hybrid phase-flow method constructs H_t on the invariant manifold M at time $t = T$ rapidly. First select a small time step $\tau > 0$, and an integer constant $K \geq 1$ such that $B = (T/\tau)^{1/K}$ is an integer power of 2.

1. Discretization. Start with a uniform or quasi-uniform grid M_h on M .
2. Initialization. Compute an approximation of H_τ .
 - (a) For each $(\mathbf{x}_0, \boldsymbol{\xi}_0) \in M_h$, $H_\tau(\mathbf{x}_0, \boldsymbol{\xi}_0)$ is computed by a discontinuous Hamiltonian solver Θ_τ described in section 2.

- (b) The value of H_τ at any other point is given via either a local interpolation or a discontinuous Hamiltonian solver Θ_τ .
3. Construct $H_{B^{k+1}\tau}$ from $H_{B^k\tau}$, loop for $b = 1, \dots, B - 1$:
- (a) For each $(\mathbf{x}_0, \boldsymbol{\xi}_0) \in M_h$

$$H_{(b+1) \cdot B^{k+1}\tau}(\mathbf{x}_0, \boldsymbol{\xi}_0) = H_{B^k\tau}(H_{b \cdot B^k\tau}(\mathbf{x}_0, \boldsymbol{\xi}_0)) \quad (23)$$

- (b) For other points, use the local interpolation or the discontinuous Hamiltonian solver Θ_τ .

The difference of this algorithm from the previous phase-flow method of Ying and Candès [26] lies in that, since the particle velocity $\boldsymbol{\xi}$ maybe discontinuous after the use of the interface solver \tilde{h} , one cannot just use the local interpolation for such discontinuous data. Instead, for such particles, we use the direct discontinuous Hamiltonian solver described in the previous section. The detailed implementation of the algorithm will be described in the next subsection.

3.2 The detailed implementation

To implement the hybrid phase-flow method, a key issue is to identify the particles that cannot be interpolated. These particles will be constructed numerically using the discontinuous Hamiltonian solver described in Section 2.

We first introduce some symbols. The basic computational domain is M .

Symbol 1 Let E_i be the smooth region separated by the interface. And we define $\mathcal{E}(\mathbf{x}, \boldsymbol{\xi}) = i$, if $(\mathbf{x}, \boldsymbol{\xi}) \in E_i$.

Symbol 2 Let $N_i^{(k)} = (\mathbf{x}_i^{(k)}, \boldsymbol{\xi}_i^{(k)}) \in M$, which is the particle initially at $N_i^{(0)} = (\mathbf{x}_i^{(0)}, \boldsymbol{\xi}_i^{(0)})$ after k iterations. Here $N_i^{(0)} = (\mathbf{x}_i^{(0)}, \boldsymbol{\xi}_i^{(0)})$ also define the mesh M_h .

Symbol 3 Let G_j denote the mesh cells, and $\mathcal{N}(G_j) = \{N_{j_1}^{(0)}, \dots, N_{j_l}^{(0)}\}$ be the set of mesh points (or vertices) associated with the mesh cell G_j , l indicates the number of mesh points (or vertices). Define $\mathcal{G}(\mathbf{x}, \boldsymbol{\xi}) = j$, if $(\mathbf{x}, \boldsymbol{\xi}) \in G_j$.

Symbol 4 Let $\mathcal{T}_k(N_i^{(0)})$ and $\mathcal{R}_k(N_i^{(0)})$ denote the number of transmissions and reflections respectively undertaken by the particle initially at $N_i^{(0)}$.

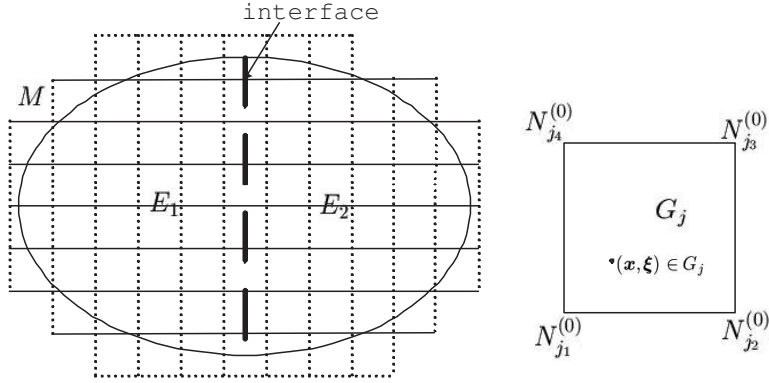


Figure 3: The mesh.

Symbol 5 Let $\mathcal{I} : \mathbb{R}^{2d(2l+1)} \rightarrow \mathbb{R}^{2d}$ denote the interpolation function, and

$$(\mathbf{y}^*, \boldsymbol{\eta}^*) = \mathcal{I} \left((\mathbf{x}^1, \boldsymbol{\xi}^1), \dots, (\mathbf{x}^l, \boldsymbol{\xi}^l), (\mathbf{y}^1, \boldsymbol{\eta}^1), \dots, (\mathbf{y}^l, \boldsymbol{\eta}^l); (\mathbf{x}^*, \boldsymbol{\xi}^*) \right). \quad (24)$$

Here \mathcal{I} interpolates at points $(\mathbf{x}^i, \boldsymbol{\xi}^i) \in \mathbb{R}^{2d}$ the values $(\mathbf{y}^i, \boldsymbol{\eta}^i) \in \mathbb{R}^{2d}$ ($i = 1, \dots, l$). For $(\mathbf{x}^*, \boldsymbol{\xi}^*)$, \mathcal{I} gives its value $(\mathbf{y}^*, \boldsymbol{\eta}^*)$.

Now we give the detailed algorithm for the hybrid phase-flow method:

1. Start with a uniform or quasi-uniform mesh $M_h = \{N_i^{(0)} | i = 1, \dots, I\}$. G_j and $\mathcal{N}(G_j)$ ($j = 1, \dots, J$) are then also defined. The stopping time is $t = T$. The small time τ and number of iteration $K \geq 1$ is selected to be satisfied $B = (T/\tau)^{1/K}$ is an integer power of 2.
2. Set $k = 0$, $\mathcal{T}_0(N_i^{(0)}) = 0$ and $\mathcal{R}_0(N_i^{(0)}) = 0$.
3. Set $k = 1$. For $i = 1, \dots, I$,

$$N_i^{(1)} = \Theta_\tau(N_i^{(0)}). \quad (25)$$

Since the discontinuous Hamiltonian solver Θ_τ can check whether the particle is transmitted or reflected during the small time interval $[0, \tau]$, we can set

$$\mathcal{T}_1(N_i^{(0)}) = \mathcal{T}_0(N_i^{(0)}) + 1, \quad \mathcal{R}_1(N_i^{(0)}) = \mathcal{R}_0(N_i^{(0)}), \quad (26)$$

for the particle transmitted, or

$$\mathcal{T}_1(N_i^{(0)}) = \mathcal{T}_0(N_i^{(0)}), \quad \mathcal{R}_1(N_i^{(0)}) = \mathcal{R}_0(N_i^{(0)}) + 1, \quad (27)$$

for the particle reflected, or

$$\mathcal{T}_1(N_i^{(0)}) = \mathcal{T}_0(N_i^{(0)}), \quad \mathcal{R}_1(N_i^{(0)}) = \mathcal{R}_0(N_i^{(0)}), \quad (28)$$

for the particle not hitting the interface.

4. For particle $N_i^{(k)}$ ($i = 1, \dots, I$), update its value at next iteration step

$$N_i^{(k+1)} = N_i^{(k)} \quad (29)$$

$$\mathcal{T}_{k+1}(N_i^{(0)}) = \mathcal{T}_k(N_i^{(0)}), \quad (30)$$

$$\mathcal{R}_{k+1}(N_i^{(0)}) = \mathcal{R}_k(N_i^{(0)}). \quad (31)$$

Loop the remain part for $b = 1, \dots, B - 1$: there exists $j = \mathcal{G}(N_i^{(k+1)})$ such that $N_i^{(k+1)} \in G_j$, for $\forall m_1 \neq m_2 \in \{j_1, j_2, \dots, j_l\}$, that is $N_{m_1}^{(0)}, N_{m_2}^{(0)} \in \mathcal{N}(G_j)$, we check the follow statements:

$$\mathcal{E}(N_{m_1}^{(0)}) = \mathcal{E}(N_{m_2}^{(0)}), \quad (32)$$

$$\mathcal{T}_k(N_{m_1}^{(0)}) = \mathcal{T}_k(N_{m_2}^{(0)}), \quad (33)$$

$$\mathcal{R}_k(N_{m_1}^{(0)}) = \mathcal{R}_k(N_{m_2}^{(0)}). \quad (34)$$

(a) If the statements are true, the particle $N_i^{(0)}$ is called a standard particle for iterative parameter group (k, b) , and we define the new value of $N_i^{(k+1)}$ by the local interpolation:

$$N_i^{(k+1)} = \mathcal{I} \left(N_{j_1}^{(0)}, \dots, N_{j_l}^{(0)}, N_{j_1}^{(k)}, \dots, N_{j_l}^{(k)}; N_i^{(k+1)} \right). \quad (35)$$

The numbers of transmission and reflection are updated as

$$\mathcal{T}_{k+1}(N_i^{(0)}) = \mathcal{T}_{k+1}(N_i^{(0)}) + \mathcal{T}_k(N_{j_1}^{(0)}), \quad (36)$$

$$\mathcal{R}_{k+1}(N_i^{(0)}) = \mathcal{R}_{k+1}(N_i^{(0)}) + \mathcal{R}_k(N_{j_1}^{(0)}). \quad (37)$$

(b) If one of the statements is false, $N_i^{(k)}$ is called a special particle for iterative parameter group (k, b) , and we define the new value of $N_i^{(k+1)}$ by the discontinuous Hamiltonian solver: loop B^k times and update the value

$$N_i^{(k+1)} = \Theta_\tau(N_i^{(k+1)}). \quad (38)$$

We also update $\mathcal{T}_{k+1}(N_i^{(0)})$ and $\mathcal{R}_{k+1}(N_i^{(0)})$ using the same idea as in step 3.

5. If $k = K$, the computation is finished, otherwise let $k = k + 1$ and go to step 4.

Remark 3 Here we emphasize that equations (32)-(34) give an approximate judgement that whether the phase flow in G_j is smooth. If statements are true, this means the phase flow in G_j is smooth and we can define the value of $N_i^{(k+1)}$ using local interpolation. Otherwise the phase flow in G_j contains discontinuities and we have to use discontinuous Hamiltonian solver to define the value of $N_i^{(k+1)}$.

Remark 4 *The criteria (32)-(34) is at least first order, this based on a simple argument: if constant potential is taken here, this judgement gives the exact solution.*

When the computation is finished, we have an approximation of all particles initially at $N_i^{(0)} (i = 1, \dots, I)$ at time $T = B^K \tau$, that is, particles with location and velocity $N_i^{(K)} (i = 1, \dots, I)$.

To approximate particles at a $2d$ -dimensional phase space lattice M_h , with N particles in each direction, the total number of ODEs will be $O(N^{2d})$. By considering the number of time steps, the total computational complexity is $O(N^{2d}L)$ with $L = B^K, T = B^K \tau$. If using hybrid phase-flow method, the computational complexity is divided into two parts. The first part is the complexity of the standard particles, which is $O(N^{2d})$ per time step. As the number of iteration is $K = O(L^{1/S})$ for the standard phase-flow method, their complexity is $O(N^{2d}L^{1/S})$. The second part is the complexity of the special particles, which is estimated as $O(N^{2d-1})$ (this will be numerically confirmed in a later section). As the time step is L , their complexity is $O(N^{2d-1}L)$. Adding these two parts, the total computational complexity for the hybrid phase-flow method is $O(N^{2d}L^{1/S} + N^{2d-1}L)$.

Remark 5 *The heuristic explanation for this estimate is that the special particles should be in one of these situations at fixed time t : (1) located within $O(\Delta \mathbf{x})$ distance from the interface at time t , (2) located within $O(\Delta \mathbf{x}, \Delta \boldsymbol{\xi})$ distance from the critical line which will match the interface after traveling with time t , (3) located within $O(\Delta \mathbf{x}, \Delta \boldsymbol{\xi})$ distance from the borderline that separate the particles transmission and reflection. All of these particles lie in a small band compare to the entire computational domain, thus gives an estimate of $O(N^{2d-1})$.*

4 Applications and numerical examples

When $H = \frac{1}{2}|\boldsymbol{\xi}|^2 + V(\mathbf{x})$, the Hamiltonian system (1)-(2) defines the bicharacteristics of the d -dimensional Liouville equation in classical mechanics:

$$f_t + \boldsymbol{\xi} \cdot \nabla_{\mathbf{x}} f - \nabla_{\mathbf{x}} V \cdot \nabla_{\boldsymbol{\xi}} f = 0, \quad t > 0, \quad \mathbf{x}, \boldsymbol{\xi} \in \mathbb{R}^d, \quad (39)$$

which describes the density distribution $f(t, \mathbf{x}, \boldsymbol{\xi}) > 0$ of classical particles at time t , position \mathbf{x} moving with velocity $\boldsymbol{\xi}$. It also arises in the high frequency limit of linear high frequency waves, see [4, 21]. The Liouville equation (39) can also be used for the level set method for the computation of multivalued solutions to quasilinear PDEs, see [2, 13].

The so-called particle method for the Liouville equation (39) is based on numerically solving the Hamiltonian system (1)-(2). For prescribed initial data

$$f(\mathbf{x}_0, \boldsymbol{\xi}_0, 0) = f_0(\mathbf{x}_0, \boldsymbol{\xi}_0), \quad (40)$$

one can obtain $f(\mathbf{x}, \boldsymbol{\xi}, T)$ through the method of characteristics,

$$f(\mathbf{x}, \boldsymbol{\xi}, T) = f_0(H_{-T}(\mathbf{x}, \boldsymbol{\xi})). \quad (41)$$

One difficulty arises in such applications, since the initial data often takes the following form

$$f(\mathbf{x}, \boldsymbol{\xi}, 0) = \rho_0(\mathbf{x})\delta(\boldsymbol{\xi} - \mathbf{u}_0(\mathbf{x})), \quad (42)$$

see for example [5, 20]. In the physical space, the moments of f :

$$\rho(\mathbf{x}, t) = \int f(\mathbf{x}, \boldsymbol{\xi}, t) d\boldsymbol{\xi} \quad (43)$$

$$\rho(\mathbf{x}, t)\mathbf{u}(\mathbf{x}, t) = \int f(\mathbf{x}, \boldsymbol{\xi}, t)\boldsymbol{\xi} d\boldsymbol{\xi} \quad (44)$$

may become multivalued [11, 23]. The level set method proposed in [12] solves the Liouville equation (39) with initial data (42) by decomposing f into ϕ and ψ_i ($i = 1, \dots, d$) where ϕ and ψ_i solve the same Liouville equation (39) with initial data

$$\phi(\mathbf{x}, \boldsymbol{\xi}, 0) = \rho_0(\mathbf{x}), \quad \psi_i(\mathbf{x}, \boldsymbol{\xi}, 0) = \xi_i - u_{i0}(\mathbf{x}), \quad (45)$$

respectively. This allows the numerical computations for a bounded solution rather than measure-valued solution of the Liouville equation with singular initial data (42), which greatly enhances the numerical resolution. The moments can be recovered through

$$\rho(\mathbf{x}, t) = \int \phi(\mathbf{x}, \boldsymbol{\xi}, t) \prod_{i=1}^d \delta(\psi_i) d\boldsymbol{\xi}, \quad (46)$$

$$\rho(\mathbf{x}, t)\mathbf{u}(\mathbf{x}, t) = \int \phi(\mathbf{x}, \boldsymbol{\xi}, t)\boldsymbol{\xi} \prod_{i=1}^d \delta(\psi_i) d\boldsymbol{\xi}. \quad (47)$$

Numerical computations of multivalued solution for smooth potential using this technique were given in [12]. It was extended for discontinuous potential in [14] using finite difference and finite volume methods. See also [24] for the discussing of delta function integrals (46)-(47). Below we will apply our hybrid phase-flow method for the level set computations of multivalued solution the physical observables ρ , $\rho\mathbf{u}$, etc.

In our numerical examples, we will compare the l^1 errors at time $t = T$ for H_{-T} , ϕ , ψ , ρ and $\rho\mathbf{u}$. To study the complexity of the algorithm, we will also give the ratio of the averaged number of the special particles over the number of total particles used for the computation. We use a second order symplectic solver $\Upsilon_{\Delta t}$ presented in [17]. For the interpolation operator \mathcal{I} , we use the second order Lagrange polynomial interpolation [22].

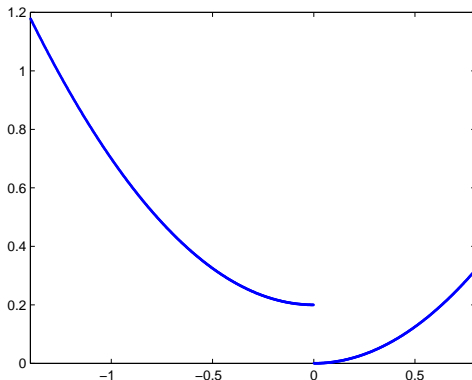


Figure 4: Example 1, potential $V(x)$.

In our computation, we use $B = 2$. In general, this version of phase flow method is unstable because it has an accuracy $O((\tau^\alpha + h^\beta)/\tau^r)$, where τ is the initial time step, h is the mesh size, α is the order of the ODE solver, β is the order of the local interpolation, and $r = \log_2(N_I)$ with N_I denoting the h -independent norm of interpolation operator. Here since we use the linear interpolation, which means $N_I = 1$, the accuracy here is $O(\tau^\alpha + h^\beta)$.

Here, the invariant domain M might be \mathbb{R}^{2d} , or

$$\left\{ (\mathbf{x}, \boldsymbol{\xi}) \in \mathbb{R}^{2d} \mid H_{\min} \leq H(\mathbf{x}, \boldsymbol{\xi}) = \frac{1}{2}|\boldsymbol{\xi}|^2 + V(\mathbf{x}) \leq H_{\max} \right\},$$

where H_{\min}, H_{\max} denote the minimal and maximal Hamiltonian in this problem.

Example 1. Consider the 1D Liouville equation

$$f_t + \xi f_x - V_x f_\xi = 0, \quad (48)$$

with discontinuous potential given by (see Figure 4)

$$V(x) = \begin{cases} \frac{1}{2}x^2 & x > 0, \\ \frac{1}{2}x^2 + 0.2 & x < 0. \end{cases} \quad (49)$$

The initial data are

$$f(x, \xi, 0) = \rho_0(x)\delta(\xi - u_0(x)) \quad (50)$$

where

$$\rho_0(x) = e^{-200(x-0.5)^2}, \quad (51)$$

$$u_0(x) = 0.4. \quad (52)$$

Table 1: the l^1 errors for different mesh sizes for Example 1

mesh	50×50	100×100	200×200	400×400
$H_{-T}(x, \xi)$	5.37×10^{-4}	2.69×10^{-4}	1.15×10^{-4}	5.58×10^{-5}
$\phi(x, \xi, T)$	7.73×10^{-4}	3.19×10^{-4}	1.21×10^{-4}	4.24×10^{-5}
$\psi(x, \xi, T)$	5.36×10^{-4}	2.71×10^{-4}	1.18×10^{-4}	5.78×10^{-5}
$\rho(x, T)$	4.16×10^{-2}	2.56×10^{-2}	1.27×10^{-2}	3.96×10^{-3}
$\rho u(x, T)$	7.85×10^{-3}	5.21×10^{-3}	2.61×10^{-3}	7.08×10^{-4}

Table 2: the errors for discontinuous Hamiltonian solver Example 1

Δt	0.04	0.02	0.01	0.005
l^1 error	1.24×10^{-4}	3.13×10^{-5}	7.87×10^{-6}	1.97×10^{-6}
l^2 error	1.50×10^{-4}	3.78×10^{-5}	9.48×10^{-6}	2.38×10^{-6}
l^∞ error	1.21×10^{-3}	3.01×10^{-4}	7.52×10^{-5}	1.88×10^{-5}

The computational domain (also the invariant manifold) is

$$M = \{(x, \xi) \in [-1, 1] \times [-1, 1] | 0 \leq H = V(x) + \frac{1}{2}\xi^2 \leq 0.4\} \quad (53)$$

We output the solutions at time $T = 3.4$, see Figures 5-6. It shows the numerical solutions of density $\rho(x, t)$ and moment $\rho u(x, t)$ with different meshes against the exact solutions.

We show the l^1 errors of H_{-T}, ϕ, ψ, ρ and ρu with different meshes on the invariant manifold M in Table 1. One can see that the numerical solution converges at about first order. Note the discontinuous Hamiltonian solver $\Theta_{\Delta t}$ is second order convergence here, see Table 2, the reason for the first order convergence comes from the criteria (32)-(34). However, this is still more accurate than the finite difference and finite volume method in [14] where only halfth order was achieved [25].

The averaged number of the special particles per iteration (NSP) and the number of total particles (NTP) used in the computation for different meshes and different time are given in Table 3. From the table, one can see that the ratio between NSP and NTP is reduced with rate of first order with reduced mesh sizes. Moreover, their ratio is almost independent of time.

Example 2. Consider the Liouville equation with the discontinuous potential given by (see Figure 7)

$$V(x) = \begin{cases} 0.5x^2 & x > 0, \\ 0.64(x+1)^2x^2 + 0.04 & x < 0. \end{cases} \quad (54)$$

Table 3: NSP versus NTP for Example 1

mesh		50×50	100×100	200×200	400×400
NTP		1178	4716	18840	75378
$t = 3.4$	NSP	153	314	620	1253
$t = 3.4$	ratio	12.99%	6.66%	3.29%	1.66%
$t = 6.8$	NSP	163	319	629	1266
$t = 6.8$	ratio	13.84%	6.76%	3.34%	1.68%
$t = 13.6$	NSP	170	345	676	1354
$t = 13.6$	ratio	14.43%	7.32%	3.59%	1.80%

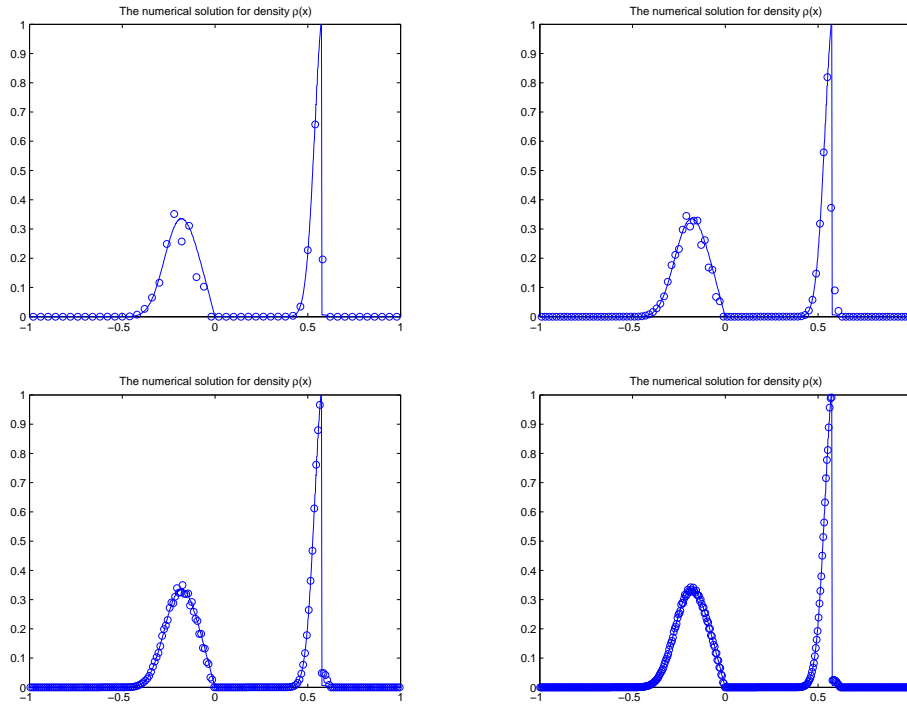


Figure 5: Example 1, density $\rho(x, t)$ at time $t = 3.4$. Solid line: the exact solutions; 'o': the numerical solutions. From upper left to lower right, the mesh is 50×50 , 100×100 , 200×200 and 400×400 .

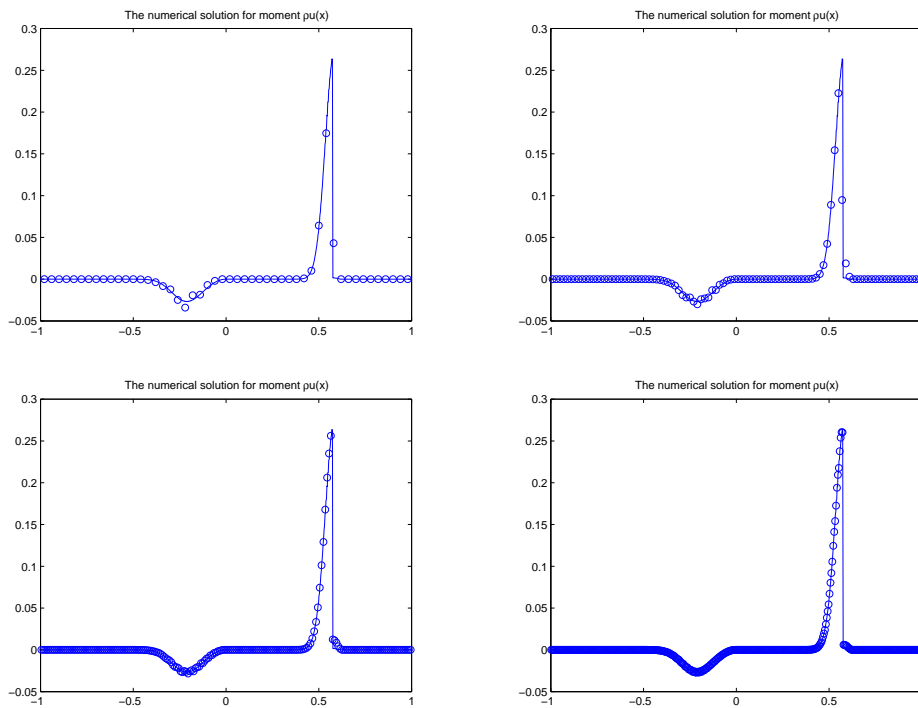


Figure 6: Example 1, moment $\rho u(x, t)$ at time $t = 3.4$. Solid line: the exact solutions; 'o': the numerical solutions. From upper left to lower right, the mesh is 50×50 , 100×100 , 200×200 and 400×400 .

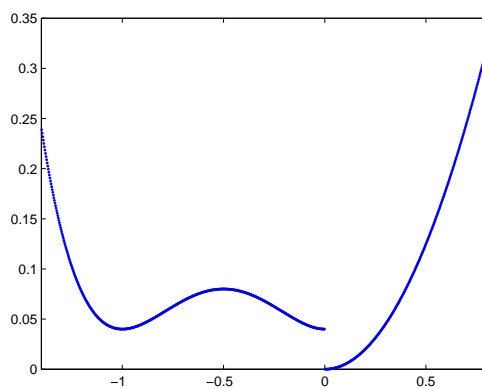


Figure 7: Example 2, potential $V(x)$.

Table 4: the l^1 errors for different meshes for Example 2

mesh	50×50	100×100	200×200	400×400
$H_{-T}(x, \xi)$	4.54×10^{-3}	1.43×10^{-3}	4.31×10^{-4}	1.31×10^{-4}
$\phi(x, \xi, T)$	3.36×10^{-3}	1.17×10^{-3}	3.67×10^{-4}	1.08×10^{-4}
$\psi(x, \xi, T)$	4.29×10^{-3}	1.34×10^{-3}	4.02×10^{-4}	1.29×10^{-4}
$\rho(x, T)$	4.49×10^{-2}	1.73×10^{-2}	7.36×10^{-3}	4.18×10^{-3}
$\rho u(x, T)$	4.56×10^{-3}	2.60×10^{-3}	1.08×10^{-3}	6.36×10^{-4}

Table 5: NSP versus NTP in Example 2

mesh	50×50	100×100	200×200	400×400
NSP	174	355	713	1454
NTP	1460	6534	26220	104810
ratio	10.61%	5.43%	2.72%	1.39%

The initial data are

$$f(x, \xi, 0) = \rho_0(x)\delta(\xi - u_0(x)) \quad (55)$$

where

$$\rho_0(x) = e^{-80\left(\frac{x-0.36}{0.4}\right)^4}, \quad (56)$$

$$u_0(x) = 0.15. \quad (57)$$

The computational domain is

$$M = \{(x, \xi) \in [-1.4, 0.8] \times [-0.7, 0.7] | 0 \leq H = V(x) + \frac{1}{2}\xi^2 \leq 0.2\}. \quad (58)$$

We output the solutions at time $T = 4$, see Figures 8-9. The 'exact' solution is a reference solution computed with a fine mesh 800×800 .

Tables 4-5 give the l^1 error of the numerical solution and the ratios NSP over NTP. We can draw the same conclusion as Example 1.

Example 3. Consider the 2D Liouville equation

$$f_t + \xi f_x + \eta f_y - V_x f_\xi - V_y f_\eta = 0, \quad (59)$$

with discontinuous potential given by

$$V(x, y) = \begin{cases} \frac{1}{2}(x^2 + y^2), & 3x + 2y > 0, \\ \frac{1}{2}(x^2 + y^2) + 0.2, & 3x + 2y < 0. \end{cases} \quad (60)$$

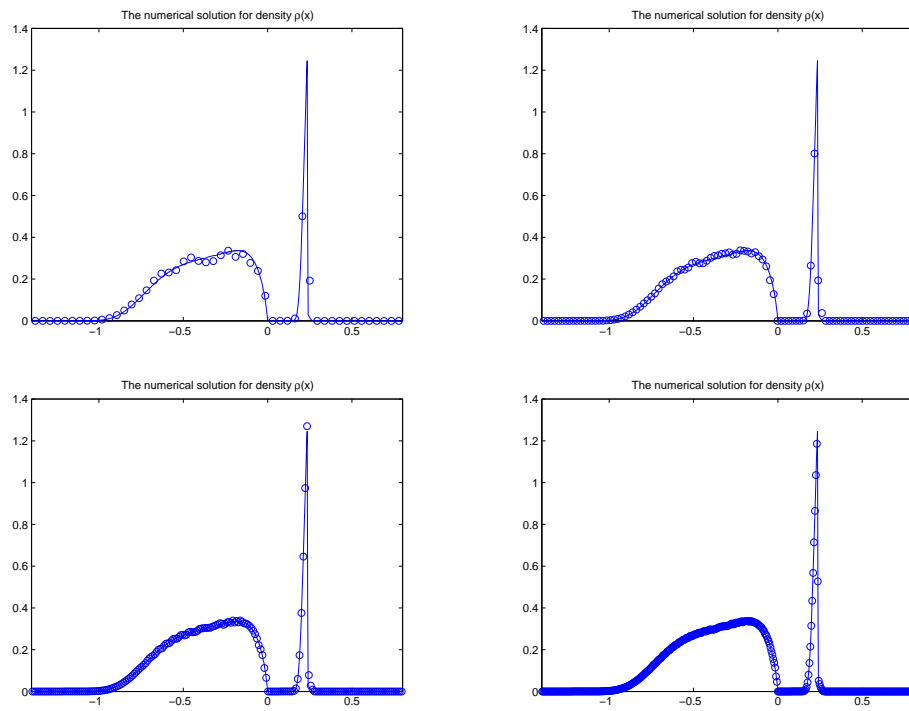


Figure 8: Example 2, density $\rho(x, t)$ at time $t = 4$. Solid line: the 'exact' solutions; 'o': the numerical solutions. From upper left to lower right, the mesh is 50×50 , 100×100 , 200×200 and 400×400 .

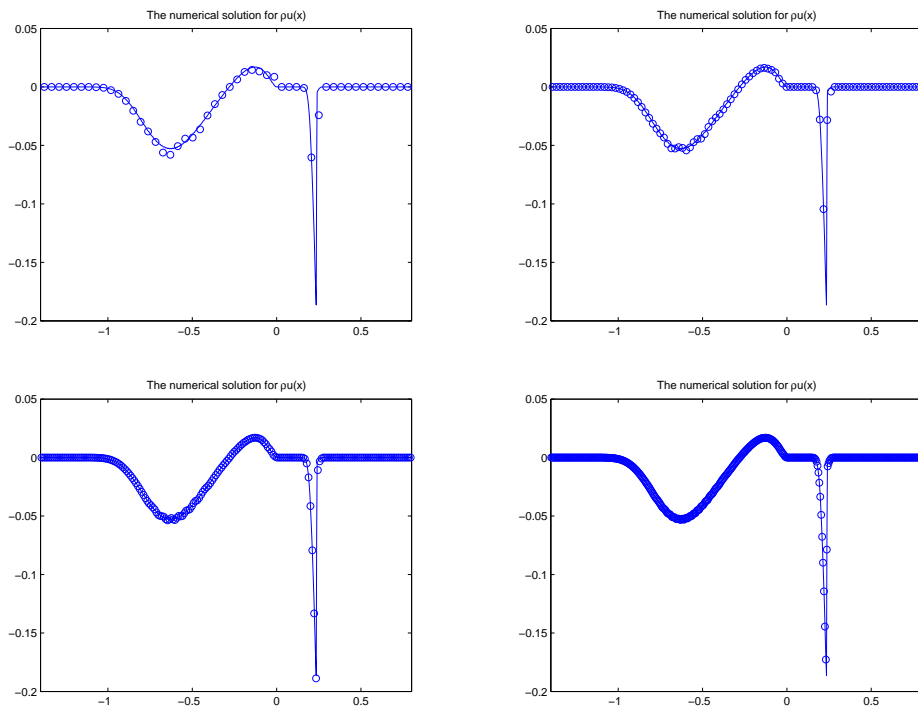


Figure 9: Example 2, momentum $\rho u(x, t)$ at time $t = 4$. Solid line: the 'exact' solutions; 'o': the numerical solutions. From upper left to lower right, the mesh is 50×50 , 100×100 , 200×200 and 400×400 .

Table 6: the l^1 errors for different meshes in Example 3

mesh	$50^2 \times 50^2$	$100^2 \times 100^2$	$200^2 \times 200^2$
$H_{-T}(x, y, \xi, \eta)$	3.39×10^{-4}	1.47×10^{-4}	5.33×10^{-5}
$\phi(x, y, \xi, \eta, T)$	3.13×10^{-4}	1.16×10^{-4}	3.60×10^{-5}
$\psi_1(x, y, \xi, \eta, T)$	4.17×10^{-4}	1.81×10^{-4}	6.52×10^{-5}
$\psi_2(x, y, \xi, \eta, T)$	3.04×10^{-4}	1.22×10^{-4}	4.36×10^{-5}
$\rho(x, y, T)$	4.89×10^{-3}	2.67×10^{-3}	1.48×10^{-3}

Table 7: NSP versus to NTP in Example 3

mesh	$50^2 \times 50^2$	$100^2 \times 100^2$	$200^2 \times 200^2$
NSP	201542	1687112	13810578
NTP	771384	12335440	197387768
ratio	26.13%	13.68%	7.00%

The initial data are

$$f(x, y, \xi, \eta, 0) = \rho_0(x, y)\delta(\xi - u_0(x, y))\delta(\eta - v_0(x, y)), \quad (61)$$

where

$$\rho_0(x, y) = e^{-5(3x+2y-1.5)^2-(2x-3y)^2}, \quad (62)$$

$$u_0(x, y) = 0.372, \quad (63)$$

$$v_0(x, y) = 0.248. \quad (64)$$

The computational domain is

$$M = \{(x, y, \xi, \eta) \in [-1, 1]^4 | 0 \leq H = V(x, y) + \frac{1}{2}\xi^2 + \frac{1}{2}\eta^2 \leq 0.4\} \quad (65)$$

We output the solutions at time $T = 3.4$, see Figure 10. It shows the numerical density $\rho(x, y, t)$ with different meshes versus the exact solutions.

The l^1 errors of numerical solutions to H_{-T} , ϕ , ψ_1 , ψ_2 and ρ with different meshes on the invariant manifold M are shown in Table 6. One can see that the numerical convergence rate is first order.

The NSP and NTP with different meshes are given in Table 7. From the table, one can see the ratio of NSP over NTP is reduced with the first order rate as the mesh size increases.

5 Conclusion

In order to describe classical particles through interfaces or barriers, Hamiltonian systems with discontinuous Hamiltonians are encountered. In this

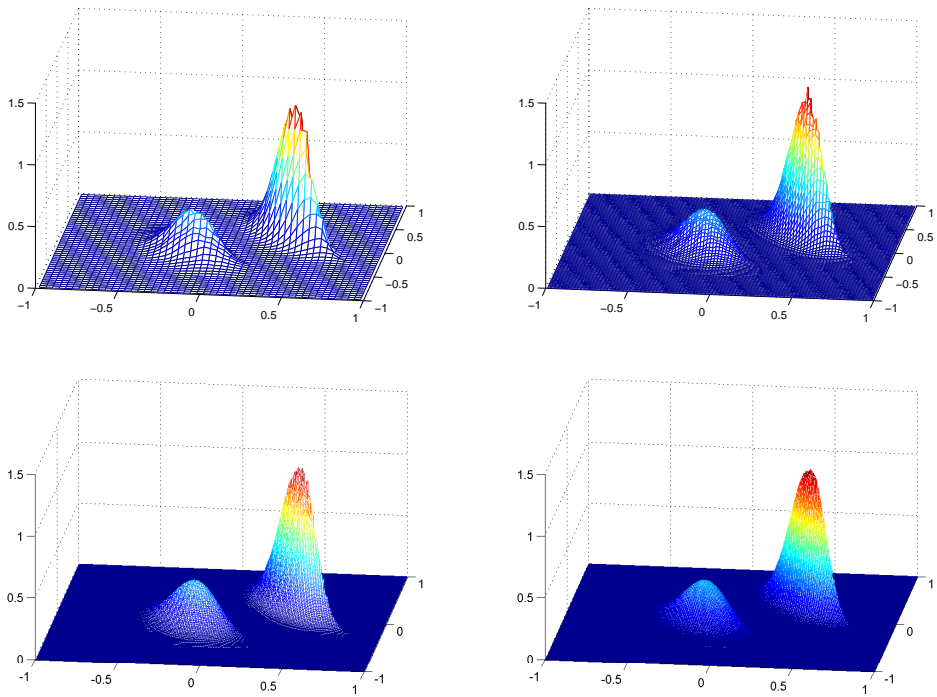


Figure 10: Example 3, density $\rho(x, y, t)$ at time $t = 3.4$ in space. Upper left: the numerical solution using $50^2 \times 50^2$ mesh; Upper right: the numerical solution using $100^2 \times 100^2$ mesh; Lower left: the numerical solution using $200^2 \times 200^2$ mesh; Lower right: the exact solution.

paper, for such Hamiltonian systems, we present a fast solver—the hybrid phase-flow method. The difference between the current method and the original phase-flow method by Ying and Candès [26] is that our method evolves the particles that undertake transmissions and reflections by a direct discontinuous Hamiltonian solver instead of the local interpolation which has poor accuracy for particles that transmit or reflect through the barriers different numbers of times. We establish a stability result for a discontinuous Hamiltonian solver originally proposed in [17] in the case of piecewise constant potentials, and use it in the hybrid phase flow method which is the new contribution here. The new method preserves the efficiency of the original phase-flow method, with a minor increase of computational cost. Numerical examples for high frequency wave problems demonstrate the efficiency and accuracy of this method.

As an alternative to the method proposed here, one may use ENO-type interpolation [7, 8] to interpolate discontinuous functions. To adequately account for the interface condition into the ENO interpolation is an issue to be addressed in a forthcoming work.

At last, we point out that boundary is an easy case for the interface. Using the similar technical proposed in our paper, we can build the phase flow on bounded domain rather than the invariant domain.

A more interesting question is how to extend the method to deal with partial transmission and reflection cases, in which one can extend the validity of the Hamiltonian systems for geometric optics and quantum wave propagation through interfaces or barriers. In this paper, our method gives an approach to the Hamiltonian system related to the classical mechanics, which have full transmissions and reflections at the barrier. This is our future work.

Acknowledgement

Hao Wu would like to thank Prof. Xin Wen for his valuable discussions, and Prof. Lexing Ying for the helpful advice on the stability issue.

References

- [1] L. Ambrosia, *Transport equation and Cauchy problem for BV vector fields*, Invent. Math. **158**, 227-260, 2004.
- [2] L.T. Cheng, H.L. Liu and S. Osher, *Computational high-frequency wave propagation using the level set method, with applications to the semi-classical limit of Schrödinger equations*, Communications in Mathematical Sciences **1** (2003), pp. 593-621.

- [3] R.J. DiPerna and P.-L. Lions, *Ordinary differential equations, transport theory, and Sobolev spaces*, Invent. Math. **98**, 511-547, 1989.
- [4] B. Engquist and O. Runborg, *Computational high frequency wave propagation*, Acta Numerica **12**, 181-266, 2003.
- [5] P. Gérard, P.A. Markowich, N.J. Mauser and F. Poupaud, *Homogenization limits and Wigner transforms*, Communications on Pure and Applied Mathematics **50** (1997), pp. 321-377.
- [6] E. Hairer, C. Lubich and G. Wanner, *Geometric Numerical Integration: Structure-preserving Algorithms for Ordinary Differential Equations*, Springer-Verlag, Berlin, 2002.
- [7] A. Harten, B. Engquist, S. Osher and S.R. Chakravarthy, *Uniformly high-order accurate essentially nonoscillatory schemes III*, Journal of Computational Physics **71** (1987), pp. 231-303.
- [8] A. Harten and S. Osher, *Uniformly high-order accurate nonoscillatory schemes I*, SIAM Journal on Numerical Analysis **24** (1987), pp. 279-309.
- [9] M.W. Hirsch, S. Smale, R.L. Devaney, *Differential Equations, Dynamical Systems, and an Introduction to Chaos*, Elsevier Academic Press, 2003.
- [10] S. Jin, *Recent computational methods for high frequency waves in heterogeneous media*, preprint.
- [11] S. Jin and X.T. Li, *Multi-phase computations of the semiclassical limit of the Schrödinger equation and related problems: Whitham vs. Wigner*, Physica D **182** (2003), pp. 46-85.
- [12] S. Jin, H.L. Liu, S. Osher and R. Tsai, *Computing multivalued physical observables for the semiclassical limit of the Schrödinger equation*, Journal of Computational Physics **205** (2005), pp. 222-241.
- [13] S. Jin and S. Osher, *A level set method for the computation of multivalued solutions to quasi-linear hyperbolic PDEs and Hamilton-Jacobi Equations*, Communications in Mathematical Sciences **1** (2003), pp. 575-591.
- [14] S. Jin and X. Wen, *Hamiltonian-preserving schemes for the Liouville equation of discontinuous potential*, Communications in Mathematical Sciences **3** (2005), pp. 285-315.
- [15] S. Jin and X. Wen, *A Hamiltonian-preserving scheme for the Liouville equation of geometrical optics with transmissions and reflections*, SIAM Journal on Numerical Analysis **44** (2006), pp. 1801-1828.

- [16] S. Jin and K. Novak, *A Semiclassical transport model for thin quantum barriers*, Multiscale Modeling and Simulation, **5** (2006), pp. 1063-1086.
- [17] S. Jin and K. Novak, *A Semiclassical Transport Model for Two-dimensional Thin Quantum Barriers*, Journal of Computational Physics **226** (2007), pp. 1623-1644.
- [18] J.B. Keller and R.M. Lewis, *Asymptotic methods for partial differential equations: the reduced wave equation and Maxwell's equations*, Surveys in applied mathematics **1** (1995), pp. 1-82.
- [19] B. Leimkuhler and S. Reich, *Simulating Hamiltonian Dynamics*, Cambridge University Press, 2004.
- [20] P.L. Lions and T. Paul, *Sur les mesures de Wigner*, Revista Matemática Iberoamericana **9** (1993), pp. 553-618.
- [21] G. Papanicolaou and L. Ryzhik, *Waves and Transport*, IAS/Park City Math. Series **5**, 305-382, 1998, L. Caffarelli and Weinan E eds.
- [22] K. Rainer, *Numerical Analysis*, Springer, New York, 1998.
- [23] C. Sparber, P.A. Markowich, N.J. Mauser, *Wigner functions versus WKB-methods in multivalued geometrical optics*, Asymptotic Analysis **33** (2003), pp. 153-187.
- [24] X. Wen, *High order numerical methods to a type of delta function integrals*, Journal of Computational Physics **226** (2007), pp. 1952-1967.
- [25] X. Wen and S. Jin, *The l^1 -error estimates for a Hamiltonian-preserving scheme to the Liouville equation with piecewise constant coefficients*, SIAM Journal on Numerical Analysis **46** (2008), pp. 2688-2714.
- [26] L.X. Ying and E.J. Candès, *The Phase flow method*, Journal of Computational Physics **220** (2006), pp. 184-215.